JACS
JOURNAL OF THE AMERICAN CHEMICAL SOCIETY

Communication

pubs.acs.org/JACS

Analysis of DNA-Guided Self-Assembly of Microspheres Using Imaging Flow Cytometry

Hao Tang,[†] Ryan Deschner,[†] Peter Allen,[‡,§] Younjin Cho,[‡,∥] Patrick Sermas,[†] Alejandro Maurer,[†] Andrew D. Ellington,[‡,§] and C. Grant Willson*[,†,‡]

[†]Department of Chemical Engineering, [‡]Department of Chemistry and Biochemistry, and [§]Institute for Cellular and Molecular Biology, The University of Texas at Austin, Austin, Texas 78712, United States

Supporting Information

ABSTRACT: Imaging flow cytometry was used to analyze the self-assembly of DNA-conjugated polystyrene microspheres. This technique enables quantitative analysis of the assembly process and thereby enables detailed analysis of the effect of structural and process variables on the assembly yield. In a demonstration of the potential of this technique, the influence of DNA strand base pair (bp) length was examined, and it was found that 50 bp was sufficient to drive the assembly of microspheres efficiently, forming not only dimers but also chainlike structures. The effect of stoichiometry on the yield was also examined. The analysis demonstrated that self-assembly of 50 bp microspheres can be driven nearly to completion by stoichiometric excess in a manner similar to Le Chatelier's principle in common chemical equilibrium.

DNA-directed self-assembly has attracted both scientific and technological interest. The use of DNA as a "smart glue" in self-assembly imparts many advantages, including high specificity,[1] thermal reversibility,[2] and modulation of assembly by factors such as nucleases,[3] competitive displacement,[4] or photo-cross-linking.[5] These advances are beginning to herald applications in a variety of fields, ranging from disease diagnosis[6] to nanoelectronics.[7,8] Most intriguingly, studies of DNA-mediated colloidal crystallization[9−11] have shown that there may be an intimate relationship between the building-block properties and the lattice parameters of the resultant self-assembled solids.

Unfortunately, it is often difficult to characterize fully the morphologies and distribution of morphologies that are created by DNA-directed assembly of particles, much less to couple the characteristics of individual particles to the yield and characteristics of larger aggregates. Many methods have been used to characterize and follow the progress of self-assembly, including UV−vis spectroscopy,[9,12] optical and fluorescence microscopy,[2−4] electron microscopy,[9,11−13] light scattering,[12,13] and X-ray diffraction.[10,11] However, these tools are largely used to characterize bulk properties rather than study individual particles in what are generally complex mixtures and distributions of assembly products and aggregates.

In this regard, flow cytometry[14] is particularly well-suited to the analysis of self-assembled clusters of micrometer-sized particles. Flow cytometry is a cell biology technique that rapidly measures the optical properties of individual cells. It gives statistically robust, quantitative counting results by measuring the scattering and/or fluorescence intensity from thousands of suspended particles as they pass one-by-one through an optical detector region. Soto et al.[15] previously used flow cytometry to estimate the assembly yield of sub-micrometer polystyrene (PS) particles. Recently, imaging flow cytometry,[16−18] a technique combining conventional flow cytometry with high-speed microscopy, has become available. Traditional cytometry gives intensity values for each particle as a function of wavelength, but imaging flow cytometry provides these data together with a fluorescence micrograph of each particle. Therefore, imaging flow cytometry analysis of DNA-guided microsphere assembly generates a detailed report describing both the number and morphology of different types of assemblies. These data enable an analysis of the details of the assembly distribution as a function of changes in the substrate, DNA sequence, reaction conditions, etc., which can provide guidance for the production of useful, large-scale assemblies.

The DNA-conjugated particles in this study were prepared via coupling of carboxylate-modified PS microspheres and amine-modified DNAs using 1-ethyl-3-(3-dimethylaminopropyl)carbodiimide (EDC). The DNA strands A and B (and also A′ and B′ and A″ and B″) are fully complementary, and their sequences are listed in Table 1. Fluorescent dyes were used to label and follow the DNAs or PS microspheres. Figure 1 depicts the construction of PS beads and their subsequent assembly, in which the polyvalent presentation of DNA on the PS microspheres generates a distribution of assemblies, including dimers, trimers, and higher-order aggregates.

Dual-color fluorescent labeling was employed, allowing different self-assembled microsphere aggregates to be readily distinguished. Figure 2a shows a double-fluorescence scatter plot and fluorescent micrographs for an experiment in which 6 μm diameter PS beads conjugated with the complementary DNA strands A and B were assembled. In the double-fluorescence scatter plot, the fluorescence intensities at two different wavelengths are plotted against each other for each particle cluster. For example, unbound A beads (blue color) reside near the x axis because they have a high Cy3 fluorescence intensity but almost zero Cy 5 intensity. Likewise, the B beads (yellow color) reside near the y axis. The A−B assemblies reside in the middle of the plot and can be further resolved into

Received: July 12, 2012
Published: August 31, 2012

   dx.doi.org/10.1021/ja3066896 | J. Am. Chem. Soc. 2012, 134, 15245−15248

Table 1. DNA Sequences (5′ → 3′)[a]

name	sequence
A	/5AmMC6/ATACG CACAT GCCTG TTT/3Cy3Sp/
B	/5AmMC6/AAACA GGCAT GTGCG TAT/3Cy5Sp/
A′	/5AmMC6/TATGC GTATG TATGC GTGCG TGCGT[b]
B′	/5AmMC6/ACGCA CGCAC GCATA CATAC GCATA[b]
A″	/56FAM/ $(AAAAA\ AAAAA)_5$/3AmMO/
B″	/5TYE665/ $(TTTTT\ TTTTT)_5$/3AmMO/
C	/56FAM/TACAT GCAGT GCGTC TTT/3AmMO/[c]

[a]The functional groups and fluorescent labels are written in the sequence format of Integrated DNA Technologies: /5AmMC6/, 5′-end amine modifier with C6 linker; /3Cy3Sp/, 3′-end Cy3 label; /3Cy5Sp/, 3′-end Cy5 label; /56FAM/, 5′-end 6-FAM label; /3AmMO/, 3′-end amine modifier; /5TYE665/, 5′-end TYE 665 label. [b]DNAs A′ and B′ do not have fluorescent labels. Instead, the fluorescent dye fluorescein cadaverine or Texas Red cadaverine was conjugated to the unreacted carboxylic acid groups on the PS microspheres after DNA conjugation. [c]Strand C is a mismatch sequence as a negative control.

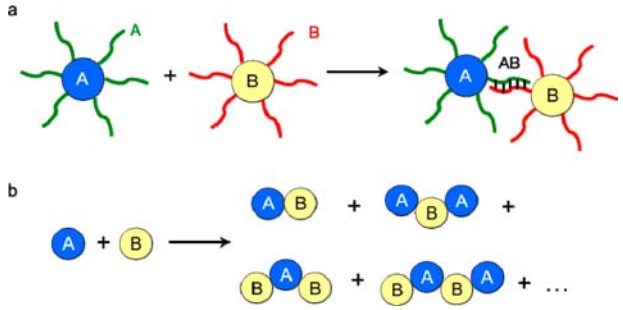

Figure 1. Assembly scheme for polyvalent polystyrene (PS) microspheres using DNA. (a) Complementary DNA strands (A and B) are conjugated onto PS microspheres. (b) The polyvalent nature of these PS microspheres yields a mixture of aggregates, including dimers (AB), trimers (A_2B and AB_2), tetramers (A_2B_2), etc. DNA strands have been omitted for clarity.

distinct subpopulations, including dimers (AB), trimers (A_2B and AB_2), and tetramers (A_2B_2). The validity of the assignments within the plot was confirmed by studying the fluorescence micrographs in Figure 2b. The yield of each type of aggregate was established in this manner. In this experiment, the assembly produced mainly dimers, with few trimer and tetramer assemblies (171 AB, 6.7%; 12 A_2B, 0.5%; 21 AB_2, 0.8%; 4 A_2B_2, 0.2%). We also noticed a significant number of homodimers (126 AA, 4.9% and 179 BB, 7.0%), which may result from the formation of secondary structures (Figure S1 and Table S1 in the Supporting Information).

It has been reported that DNA complementarity as short as 12 bp is adequate to drive the assembly of 1 and 2 μm beads.[19] While fully complementary 18 bp strands A and B can drive the assembly of 6 μm beads in a static fluorescence microscopy setup (Figure S2), the 18 bp complement provides only a low assembly yield in flow cytometry. The majority of the assembly products fail to survive the shearing force in the flow environment. These data provide important input to those who are designing large macroscopic structures that are to be generated by DNA-mediated self-assembly.

Imaging flow cytometry was used to investigate the effect of DNA length and melting point on the assembly yield; these data are summarized in Table 2. The melting point of the 25 bp DNA pair A′−B′ is 17 °C higher than that of the 18 bp A−B

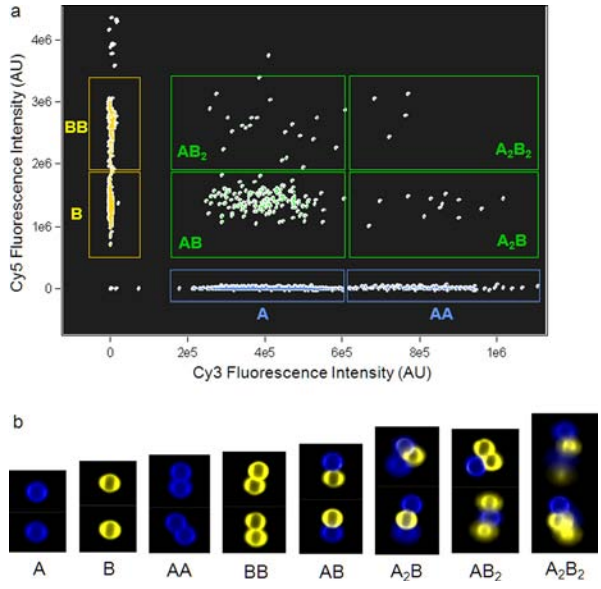

Figure 2. (a) Imaging flow cytometry chart for the assembly of 6 μm diameter PS beads. The beads were conjugated with DNA strands A (Cy3 fluorophore, blue color) and B (Cy5 fluorophore, yellow color). The fluorescence intensities have been compensated to remove the coupling due to spectral overlap and free DNA hybridization (Figure S4). (b) Representative fluorescence micrographs of beads in each assigned region.

Table 2. DNA Length and Assembly Yield[a]

DNA pair	length (bp)	mp (°C)[b]	yield (%)[c]
A + B	18 + 18	41	8.4
A′ + B′	25 + 25	58	59.5
A″ + B″	50 + 50	56	58.8
B″ + C	50 + 18	NA	0.7

[a]The diameter of microspheres was 6 μm, and their stoichiometry was 1:1. [b]The DNA melting point was calculated using the NUPACK online server[20] at a DNA concentration of 10 pM and a Na^+ concentration of 0.1 M. [c]Defined as the number of A−B assemblies divided by the total number of particles. Let A_mB_n denote a bead assembly containing m A beads and n B beads ($m, n \geq 1$). Then yield = (number of A_mB_n)/(number of A_mB_n + number of A_m + number of B_n).

pair. Increasing the melting point increased the assembly yield from 8.4 to 59.5% (Figure S3). Interestingly, the 50 bp polyadenosine and polythymidine DNA pairing, A″−B″, which has a melting point very close to that of A′−B′, gave a nearly identical assembly yield (58.8%). The DNA melting point seems to be an important factor that should be considered in the design of DNA-guided self-assembly of microspheres.

As shown in Figure 3a, the population of dimer pairs of the 50 bp A″−B″ microsphere beads (58.8%) was more than twice those of the unbound A″ and B″ beads (21.3 and 19.9%, respectively). Some higher-order assemblies were observed, including chains with lengths of ≥7 beads. Through examination of the fluorescent micrographs (Figure 3b), flow cytometry enabled verification of the fact that these chains had a precise, alternating arrangement of the two beads. It is important to report that as expected, mixtures of beads with noncomplementary sequences showed very little binding to one another (Table 2 and Figure S5). The fact that the majority of the higher-order assemblies generated in these experiments were chainlike rather than spherical may be the result of the

dx.doi.org/10.1021/ja3066896 | J. Am. Chem. Soc. 2012, 134, 15245−15248

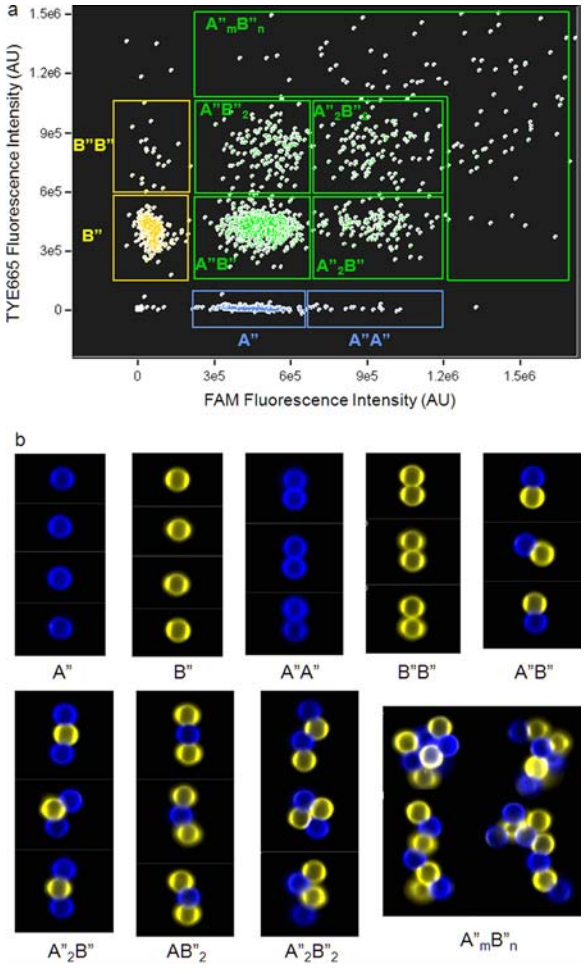

Figure 3. (a) Imaging flow cytometry chart for the assembly of 6 μm diameter PS beads. The DNA strands were A″ (FAM fluorophore, blue color) and B″ (TYE 665 fluorophore, yellow color). The $A''_mB''_n$ region extends beyond the top-right corner, and only part of the region is shown here for clarity. (b) Representative fluorescence micrographs of beads in each assigned region.

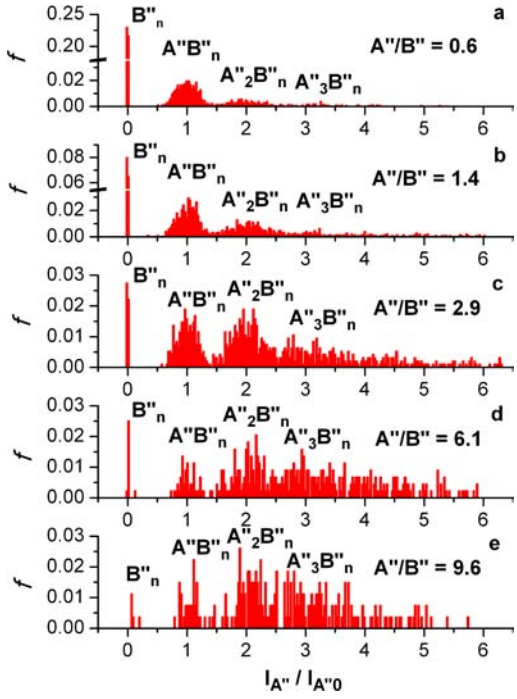

Figure 4. FAM fluorescence intensity histogram of assembly products from 6 μm A″ and 6 μm B″ beads at various A″/B″ ratios: (a) 0.6, (b) 1.4, (c) 2.9, (d) 6.1, (e) 9.6. f denotes the relative frequency, $I_{A''}$ the FAM fluorescence intensity, and $I_{A''0}$ the average FAM fluorescence intensity of the A″ monomer. The ratio $I_{A''}/I_{A''0}$ roughly indicates the number of A″ beads in a particular bead assembly.

shear fields generated in the flow channels of the imaging flow cytometer.[21]

The stoichiometric ratio of A beads to B beads was controlled to be 1:1 in the experiments above. We found that an excess of A or B can drive the assembly nearly to completion in a manner similar to Le Chatelier's principle. Figure 4 shows the change in assembly populations that occurred when different ratios of 6 μm A″ and B″ beads were mixed. At an A″/B″ ratio of 0.6, the incorporation of B″ into assemblies was 54.9%, while at an A″/B″ ratio of 9.6, the incorporation of B″ increased to 98.1% (Table S2). Increasing the A″/B″ ratio also had a profound effect on the structure of the assembly. When the A″/B″ ratio was close to 1, the major population of the assembly was $A''B''_n$ (Figure 4a,b). As the A″/B″ ratio increased, the population of $A''_2B''_n$ and $A''_3B''_n$ began to exceed that of $A''B''_n$ (Figure 4c) and finally became predominant (Figure 4d,e).

The imaging flow cytometer was also used to study variations in the assembly of structures created by mixing beads of different sizes. As shown in Figure 5, when 6 μm A″ beads were mixed with 3 μm B″ beads in a ratio of 1:10, a different aggregate structure formed, with A″ beads binding to multiple B″ beads. The average coordination number of A″ beads bound to B″ beads was 3.2. In contrast, when 6 μm A″ and 6 μm B″ beads were assembled in a 1:1 ratio (Figure 3), the average coordination number was 1.0, but when they were assembled in a 9.6:1 ratio (Figure 4), the average coordination number was 2.3. The high coordination number in Figure 5 is the result of both the heterogeneous bead size and the stoichiometric excess.

The increased coordination number suggests that DNA-guided self-assembly systems tend to maximize the total number of DNA hybridization events, which is consistent with the guidelines proposed by Mirkin and co-workers in nanoscale DNA-guided crystallization.[11] Nevertheless, self-assembly at the mesoscale (micrometer level) engenders more challenges. Both gravity and flow-induced kinetic energy increase as the third power of the particle size, while the DNA hybridization energy scales with the surface area (i.e., the second power of the particle size). Therefore, mesoscale DNA-guided self-assembly requires stronger DNA hybridization interactions.

DNA-guided crystallization can enable new technologies such as self-assembled photonic crystals. In addition, the ability to synthesize and characterize libraries of particles with faces that are substituted with varying DNA sequences provides access to another broad spectrum of applications. For example, the porous nature of a microsphere assembly provides a path for the creation of new low-k dielectric materials for microelectronics.[22] Self-assembled amorphous materials are also receiving a great deal of attention as battery electrodes[23] and hydrogen storage materials.[24] Although the DNA-coated PS microspheres described in this study are isotropic and as such do not impart orientational control, the recent advances in Janus particle fabrication[25,26] promise control of more complex mesoscale particle assemblies in the near future. The rate of

dx.doi.org/10.1021/ja3066896 | J. Am. Chem. Soc. 2012, 134, 15245−15248

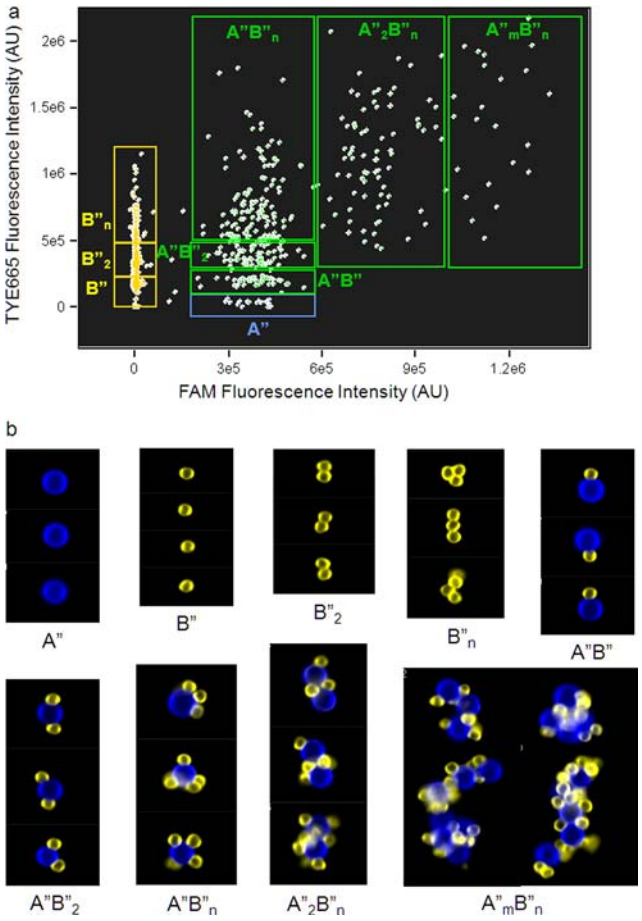

Figure 5. (a) Imaging flow cytometry chart for assembly of 6 μm diameter A″ beads and 3 μm B″ beads. The ratio of B″ beads to A″ beads was 10:1. The $A''_mB''_n$ region extends beyond the top-right corner, and only part of the region is shown here for clarity. (b) Representative fluorescence micrographs of beads in each assigned region.

progress toward that end can be significantly increased through use of imaging flow cytometry as an analytical tool.

■ ASSOCIATED CONTENT

Ⓢ Supporting Information

Experimental procedures for the DNA conjugation, flow cytometry methods, additional cytometry charts, and fluorescence microscopy images. This material is available free of charge via the Internet at http://pubs.acs.org.

■ AUTHOR INFORMATION

Corresponding Author

willson@che.utexas.edu

Present Address

[‖]Semiconductor Materials R&D Center, Cheil Industries Inc., Samsung, 332-2 Gocheon-Dong, Uiwang-Si, Gyeonggi-Do 437-711, Korea.

Notes

The authors declare no competing financial interest.

■ ACKNOWLEDGMENTS

The authors thank the UT Genome Sequencing and Analysis Facility for the equipment support and Dr. Xi Chen and Dr. Aleksandr Miklos for fruitful discussions. This work was supported by the Rashid Engineering Reagents Chair, a National Security Science and Engineering Faculty Fellowship (FA9550-10-1-0169), the National Institutes of Health (1 R01 GM094933-01), the Welch Foundation (F-1654), and the Virginia and Ernest Cockrell, Jr. Fellowship in Engineering.

■ REFERENCES

(1) Rothemund, P. W. *Nature* **2006**, *440*, 297.
(2) Valignat, M. P.; Theodoly, O.; Crocker, J. C.; Russel, W. B.; Chaikin, P. M. *Proc. Natl. Acad. Sci. U.S.A.* **2005**, *102*, 4225.
(3) Tison, C. K.; Milam, V. T. *Biomacromolecules* **2008**, *9*, 2468.
(4) Tison, C. K.; Milam, V. T. *Langmuir* **2007**, *23*, 9728.
(5) Rajendran, A.; Endo, M.; Katsuda, Y.; Hidaka, K.; Sugiyama, H. *J. Am. Chem. Soc.* **2011**, *133*, 14488.
(6) Storhoff, J. J.; Elghanian, R.; Mucic, R. C.; Mirkin, C. A.; Letsinger, R. L. *J. Am. Chem. Soc.* **1998**, *120*, 1959.
(7) Keren, K.; Berman, R. S.; Buchstab, E.; Sivan, U.; Braun, E. *Science* **2003**, *302*, 1380.
(8) Maune, H. T.; Han, S.-p.; Barish, R. D.; Bockrath, M.; Goddard, W. A., III; Rothemund, P. W. K.; Winfree, E. *Nat. Nanotechnol.* **2010**, *5*, 61.
(9) Mirkin, C. A.; Letsinger, R. L.; Mucic, R. C.; Storhoff, J. J. *Nature* **1996**, *382*, 607.
(10) Nykypanchuk, D.; Maye, M. M.; van der Lelie, D.; Gang, O. *Nature* **2008**, *451*, 549.
(11) Macfarlane, R. J.; Lee, B.; Jones, M. R.; Harris, N.; Schatz, G. C.; Mirkin, C. A. *Science* **2011**, *334*, 204.
(12) Maye, M. M.; Nykypanchuk, D.; Cuisinier, M.; van der Lelie, D.; Gang, O. *Nat. Mater.* **2009**, *8*, 388.
(13) Tikhomirov, G.; Hoogland, S.; Lee, P. E.; Fischer, A.; Sargent, E. H.; Kelley, S. O. *Nat. Nanotechnol.* **2011**, *6*, 485.
(14) Shapiro, H. M. *Practical Flow Cytometry*, 4th ed.; Wiley: Hoboken, NJ, 2003.
(15) Soto, C. M.; Srinivasan, A.; Ratna, B. R. *J. Am. Chem. Soc.* **2002**, *124*, 8508.
(16) Bonetta, L. *Nat. Methods* **2005**, *2*, 785.
(17) Basiji, D. A.; Ortyn, W. E.; Liang, L.; Venkatachalam, V.; Morrissey, P. *Clin. Lab. Med.* **2007**, *27*, 653.
(18) Helguera, G.; Rodríguez, J. A.; Luria-Pérez, R.; Henery, S.; Catterton, P.; Bregni, C.; George, T. C.; Martínez-Maza, O.; Penichet, M. L. *J. Immunol. Methods* **2011**, *368*, 54.
(19) Milam, V. T.; Hiddessen, A. L.; Crocker, J. C.; Graves, D. J.; Hammer, D. A. *Langmuir* **2003**, *19*, 10317.
(20) Zadeh, J. N.; Steenberg, C. D.; Bois, J. S.; Wolfe, B. R.; Pierce, M. B.; Khan, A. R.; Dirks, R. M.; Pierce, N. A. *J. Comput. Chem.* **2011**, *32*, 170.
(21) Rabideau, B. D.; Bonnecaze, R. T. *Langmuir* **2007**, *23*, 10000.
(22) Volksen, W.; Miller, R. D.; Dubois, G. *Chem. Rev.* **2010**, *110*, 56.
(23) Wang, H.; Wu, Y.; Bai, Y.; Zhou, W.; An, Y.; Li, J.; Guo, L. *J. Mater. Chem.* **2011**, *21*, 10189.
(24) Jeon, Y.-M.; Armatas, G. S.; Heo, J.; Kanatzidis, M. G.; Mirkin, C. A. *Adv. Mater.* **2008**, *20*, 2105.
(25) Jiang, S.; Chen, Q.; Tripathy, M.; Luijten, E.; Schweizer, K. S.; Granick, S. *Adv. Mater.* **2010**, *22*, 1060.
(26) Nie, Z.; Li, W.; Seo, M.; Xu, S.; Kumacheva, E. *J. Am. Chem. Soc.* **2006**, *128*, 9408.